Flow fields in soap films: Relating viscosity and film thickness

V. Prasad and Eric R. Weeks
Department of Physics, Emory University, Atlanta, Georgia 30322, USA
(Received 9 May 2009; published 19 August 2009)

We follow the diffusive motion of colloidal particles in soap films with varying h/d, where h is the thickness of the film and d is the diameter of the particles. The hydrodynamics of these films are determined by looking at the correlated motion of pairs of particles as a function of separation R. The Trapeznikov approximation [A. A. Trapeznikov, *Proceedings of the 2nd International Congress on Surface Activity* (Butterworths, London, 1957), p. 242] is used to model soap films as an effective two-dimensional (2D) fluid in contact with bulk air phases. The flow fields determined from correlated particle motions show excellent agreement with what is expected for the theory of 2D fluids for all our films where $0.6 \leq h/d \leq 14.3$, with the 2D shear viscosity matching that predicted by Trapeznikov. However, the parameters of these flow fields change markedly for thick films ($h/d > 7 \pm 3$). Our results indicate that three-dimensional effects become important for these thicker films, despite the flow fields still having a 2D character.

DOI: 10.1103/PhysRevE.80.026309 PACS number(s): 47.57.Bc, 68.15.+e, 87.16.D−, 87.85.gf

I. INTRODUCTION

The motion of a particle in a viscous fluid causes a flow field to be created, that is, fluid mass is displaced in a very specific manner around the particle. The nature of this flow field depends sensitively on the geometry, the boundary conditions, and the dimensionality of the system in question. For instance, flow fields in three dimensions decay as $1/R$ in an unbounded fluid, where R is the distance from the localized perturbation. On the other hand, in a two-dimensional (2D) fluid such as a thin film, flow fields decay logarithmically with distance [1–3]. One example of a 2D system exhibiting such long-range behavior under certain specific circumstances is that of soap films [4–6]. A soap film in its simplest form consists of a thin fluid layer of thickness h buffered from air phases above and below it by surfactant layers. The fluid layer has a three-dimensional (3D) shear viscosity η_{3D}, and the surfactant layers have a 2D shear viscosity η_{int} [7,8]. However, because of the finite thickness of the fluid layer, and the 2D nature of the surfactant layers, it is unclear whether a soap film should be regarded as a 2D or a 3D fluid for arbitrary film thicknesses and 3D and 2D shear viscosities.

Two-particle microrheology [9,10] provides a powerful technique to determine the flow fields in soap films. This technique has been used with great success to characterize the rheological and the flow properties of 3D systems such as biomaterials [11], polymer solutions [12,13], and biological cells [14]. To a lesser extent, it has also been used to determine the surface rheological properties of 2D fluids such as protein monolayers at an air-water interface [15]. Briefly, this technique looks at the correlated motions of particles in the system of interest. When a particle undergoes motion in the system, either by thermal excitation [9,15] or by an external perturbation [4,12], it creates a flow field in the surrounding medium. This flow field affects the motion of other particles in its vicinity. Therefore, by measuring the correlated motions of pairs of particles as a function of their separation R, the flow field in the system can be determined.

In this paper, we look at the flow fields in soap films of different thicknesses h and 3D viscosities η_{3D}, while keeping the 2D shear viscosity η_{int} constant. We embed probe particles of size d in these soap films and are able to vary the dimensionless parameter h/d by over an order of magnitude, from $h/d=0.6$ to 14.3 [16]. In order to account for the effects of the surfactant-laden interfaces and the thin fluid layer, we use the Trapeznikov approximation [17] that models the soap film as an effective interface with an effective 2D shear viscosity $\eta_T = \eta_{3D} h + 2\eta_{int}$. The flow fields in these films are then mapped as a function of R and compared to theoretical models of soap film flow. Excellent agreement is obtained between the theoretical models and the flow fields in *all* soap films, irrespective of the parameter h/d, using η_T. However, we find that single-particle motion is faster than expected for thicker films with $h/d > 7 \pm 3$. This leads us to state that the hydrodynamics of the soap films transition from 2D- to 3D-like behavior at this particular value of h/d.

II. EXPERIMENTS

A. Preparation of soap films

Soap films are prepared from mixtures of water, glycerol, and surfactants that stabilize the interfaces. By changing the ratio of water and glycerol, the viscosity η_{3D} of the soap solution is controlled. The surfactants used in this study are obtained from the commercially available dishwashing detergent brand Dawn. Known quantities of this detergent are added to the water/glycerol mixture to create the soap solutions. The chemical formulation of Dawn is proprietary and hence cannot be determined; however, for all the soap films in this study we use the same amount of dishwashing detergent (2% by weight) to ensure consistency.

Fluorescent polystyrene spheres (Molecular Probes, carboxylate modified, $d=210$ or 500 nm) are added to the soap solutions. The soap films are created by dipping a circular stainless steel frame of thickness 1 mm into the solutions and drawing it out gently. The frame is then enclosed in a chamber designed to maintain relative humidity and minimize convective drift. The particles are then imaged with fluorescence microscopy to determine their motion in real space and real time.

B. Particle tracking by fluorescence microscopy

The tracer particles are imaged in a fluorescent microscope at a frame rate of 30 Hz, with a 20× objective (numerical aperture=0.4, resolution=465 nm/pixel) used for large particles (d=500 nm) and with a 40× objective (numerical aperture=0.55, resolution=233 nm/pixel) for smaller (d=210 nm) particles. For each sample, short movies with a duration of ~30 s are recorded with a charge-coupled device camera that has a 640×486 pixel resolution, with hundreds of particles lying within the field of view. The movies are later analyzed by particle tracking to obtain the positions of the tracers [18]. From the particle positions, we determine their vector displacements by the relation $\Delta r(t,\tau)=r(t+\tau)-r(t)$, where t is the absolute time and τ is the lag time. Any global motion is subtracted from these vector displacements to minimize the effects of convective drift caused by the air phases that contact the soap film [19]. These vector displacements are then used to determine the mean-square displacement (MSD), $\langle \Delta r^2(\tau)\rangle$, where the average is performed over all particles and all times t. Correlated motions of particles [9,20] are also determined by looking at the products of particle displacements, which we describe in Sec. III in greater detail.

C. Determination of soap film thickness

The thickness of the soap films in this study ranges from $h\sim 300$ nm to 3 μm, which is close to the wavelength of visible light. This makes the spectroscopic technique of optical interference the most viable option for determining the thickness of these films. Immediately after taking each movie, the film is transferred to a spectrophotometer and its thickness h determined from the transmitted intensity [21]. We briefly describe the details of this technique: two light rays of the same wavelength passing through a thin film will interfere with each other. This interference will be constructive or destructive, depending on whether one light ray has traveled an integer or a half-integer multiple of the wavelength with respect to the other ray. The light transmitted through the film will have a minimum (or the absorption will have a maximum) when

$$(2n\cos\theta)h=(m+1/2)\lambda, \tag{1}$$

where n is the index of refraction of the film, λ is the wavelength of light, θ is the angle of incidence (typically, θ=0°), and m is a non-negative integer. If $\lambda_{pk,1}$ and $\lambda_{pk,2}$ are two successive maxima (or minima) in the transmitted light, then the thickness of the film can be easily determined by the relation [21]

$$h=\frac{1}{2n}\left[\frac{1}{\lambda_{pk,1}}-\frac{1}{\lambda_{pk,2}}\right]^{-1}. \tag{2}$$

Figure 1 demonstrates how the thickness of a soap film is determined in practice. It shows the absorption spectrum for a soap film (50/50 water/glycerol mixture with 2% Dawn) that has been placed in a uv–visible spectrophotometer (Agilent Technologies, Santa Clara, CA). The spectrum shows multiple maxima and minima because of constructive and destructive interferences as light rays traverse through the soap film. By substituting the values of the two successive maxima $\lambda_{pk,1}$=409 nm and $\lambda_{pk,2}$=576 nm in Eq. (2) and n=1.4 for a 50/50 water/glycerol mixture, the thickness h=504 nm of the soap film can be estimated. We then average the value of h obtained by repeating this process for all the successive peaks observed in the spectrum, giving us h=510±10 nm for this particular soap film.

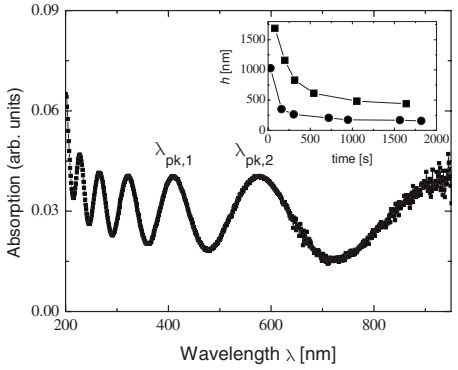

FIG. 1. Absorption spectrum of a soap film (50/50 water/glycerol mixture, 2% Dawn by weight) as a function of normally incident wavelength of light. From the peaks in this spectrum and Eq. (2), the thickness of the film is inferred to be h=510 nm. Inset: the time dependence of h for two different soap films prepared with 60:40 water/glycerol ratio and 2% concentration of Dawn.

The inset to Fig. 1 shows a time series of film thickness for two soap films comprised of a 60/40 water/glycerol mixture with 2% Dawn as surfactant. It is evident from the figure that both films thin rapidly over an initial time scale of ~500 s, but rapidly equilibrate to a quasisteady state over longer time scales where relatively small changes are seen in the thickness. Care is taken in our measurements to ensure that the particle trajectories are recorded after this initial transient period. This has the added advantage that convective drift of the tracers is also substantially reduced beyond 500 s, resulting in more accurate measurements of particle motions.

III. THEORY

A soap film is considered "thin" when the thickness h of the film is comparable to the particle size d. In fact, it has been shown that thin films behave as a 2D fluid [5,16]. This assumption can be justified by modeling the soap film, with its two interfaces and a thin fluid layer, as a single effective interface in contact with two bulk air phases [17] (see Fig. 2). The effective interface then has an effective 2D shear viscosity η_T, which is given by

$$\eta_T=\eta_{3D}h+2\eta_{\rm int}, \tag{3}$$

where $\eta_{\rm int}$ is the 2D shear viscosity of the two surfactant-laden interfaces and η_{3D} is the viscosity of the liquid within the film. One immediate consequence of this approximation is that a tracer particle in a soap film must diffuse as though embedded in an interface in contact with bulk air phases. According to Saffman and Delbrück [22], this diffusion follows the equation

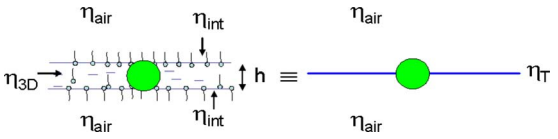

FIG. 2. (Color online) Schematic of the Trapeznikov approximation, where the entire soap film is approximated as a single interface in contact with bulk air phases. Reproduced and modified with permission from [16].

$$\langle \Delta r^2 \rangle = \frac{k_B T}{\pi \eta_{SD}} \left[\ln\left(\frac{2\eta_{SD}}{\eta_{\text{air}} d} \right) - \gamma_E \right] \tau, \tag{4}$$

where η_{air} is the viscosity of the air phase and $\gamma_E = 0.577$ is Euler's constant. It is expected that $\eta_{SD} = \eta_T$ and indeed this has been found to be true for thin films [16]; the limits of this for thick films will be discussed in Sec. IV.

The other consequence of the Trapeznikov approximation is that the hydrodynamics of a soap film must mimic that of a 2D fluid. To probe the hydrodynamics, we look at the correlated motions of particles embedded in the soap film. Similar to the treatment in [4], we measure correlated and anticorrelated coupled displacements of particles to determine the "eigenmodes" of particle motion in a 2D fluid. We give here a brief description of the method used by Di Leonardo *et al.* [4]. They actively perturbed pairs of particles by means of optical tweezers in a soap film. The displacements of the particles from their mean particle positions are then determined. These displacements are related to the strength of the trap and the mobility of the particles. The mobility of each particle is affected by the presence of the other particle and therefore contains information about the nature of the flow fields in the soap film. The two-dimensional Stokes equation can then be solved and the resulting motions of the particles decomposed into eigenmodes of motion. There are four such eigenmodes in 2D given by $\lambda_{x\pm}$ and $\lambda_{y\pm}$, where x, y represent the motion parallel and perpendicular to the lines joining the centers of the particles and $\pm$ represent rigid motions and relative displacements, respectively. These mobilities are given by the equations

$$\lambda_{x\pm} = b\left[1 \pm \frac{1}{4\pi \eta_{3\text{D}} hb} \ln\left(\frac{L}{R} \right) \right],$$

$$\lambda_{y\pm} = b\left\{ 1 \pm \frac{1}{4\pi \eta_{3\text{D}} hb} \left[\ln\left(\frac{L}{R} \right) - 1 \right] \right\}, \tag{5}$$

where R is the separation between the particles, L is a characteristic length scale, and b has units of mobility (kg^{-1} s). This length scale L demands some explanation; flow fields in 2D are long ranged and tend to diverge because of the presence of the logarithmic terms in Eqs. (5). This divergence is cut off due to the presence of a length scale L, which has many possible origins. Some of these include finite size of the film, inertial effects, and viscous drag on the interfaces from the surrounding bulk fluid phases (air). In the subsequent sections, we will look at a series of soap films with different material parameters ($\eta_{3\text{D}}$, h) and discuss in detail the origin of this length scale L. A detailed derivation of Eqs. (5) can also be found in Ref. [4]. It is clear from Eqs. (5) that the mobilities of the particles split around a mean mobility b, with rigid motions (+) being favored and relative displacements (−) being opposed. The hydrodynamic interactions between the particles are also governed by the fluid layer of the film, shown by the appearance of $\eta_{3\text{D}} h$ in the equation.

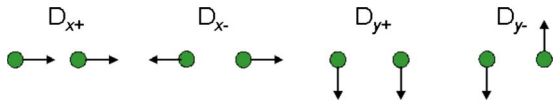

FIG. 3. (Color online) Coupled motions of particles embedded in the soap films. There are four possible eigenmodes associated with this coupling, correlated and anticorrelated motion parallel ($D_{x\pm}$) and perpendicular ($D_{y\pm}$) to the lines joining the centers of the particles.

Our approach to determine the flow fields in soap films, while analogous to the approach of Di Leonardo *et al.*, has some important differences. We measure the correlated *thermal* motions of pairs of particles embedded in the soap films. There are four such eigenmodes in 2D, represented by $D_{x\pm}$ and $D_{y\pm}$, which correspond to the longitudinal and the transverse components of coupled motion, with $\pm$ representing correlated and anticorrelated motions, respectively, as shown in Fig. 3. The correlation functions are given by [23,24]

$$D_{x\pm}(R,\tau) = \left\langle \tfrac{1}{2}[\Delta r_x^i(\tau) \pm \Delta r_x^j(\tau)]^2 \delta(R - R^{ij}) \right\rangle_{i \neq j},$$

$$D_{y\pm}(R,\tau) = \left\langle \tfrac{1}{2}[\Delta r_y^i(\tau) \pm \Delta r_y^j(\tau)]^2 \delta(R - R^{ij}) \right\rangle_{i \neq j}, \tag{6}$$

where i, j are particle indices, the subscripts x and y represent the motion parallel and perpendicular to the line joining the centers of particles, and R^{ij} is the separation between particles i and j. The average is performed over all possible pairs of particles with a given separation R. This has the advantage of averaging out correlations from other particles that are not part of the pair. We are therefore confident that many-body effects due to the presence of other particles are minimized in our correlation functions. Similar to [15], we observe that $D_{x\pm}, D_{y\pm} \sim \tau$, which enables the estimation of four τ-independent quantities $\langle D_{x\pm}/\tau \rangle_\tau$ and $\langle D_{y\pm}/\tau \rangle_\tau$ depending only on R and having units of a diffusion constant. In this paper, we shall discuss only these τ-independent quantities.

These τ-independent correlation functions have a physical interpretation; for instance, $\langle D_{x+}/2\tau \rangle_\tau$ is the diffusion constant of the center of mass of the particle pairs along the line joining their centers, while $\langle D_{x-}/2\tau \rangle_\tau$ is the diffusion constant of the interparticle separation. Our correlation functions can then be related to eigenmobilities of Di Leonardo *et al.* by the relations

$$\langle D_{x\pm}/\tau \rangle = 2k_B T \lambda_{x\pm},$$

$$\langle D_{y\pm}/\tau \rangle = 2k_B T \lambda_{y\pm}. \tag{7}$$

From Eqs. (5), we can then derive theoretical expressions for our thermally driven correlation functions which are given by

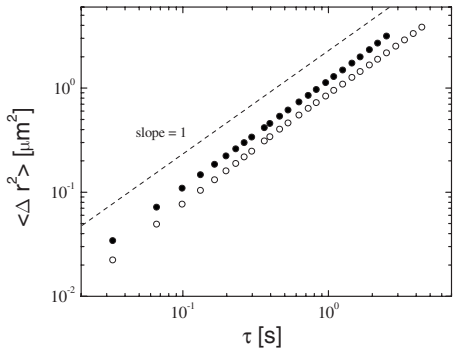

FIG. 4. MSD for a soap film, sample (f) in Table I (solid circles), compared to MSD in a bulk solution that comprises the fluid layer of the soap film (open circles). Dashed line shows a slope of 1, indicating free diffusion. The effective 2D shear viscosity of the film can be evaluated from Eq. (4) and is given by η_{SD} =8.03 nPa s.

$$\langle D_{x\pm}/\tau\rangle = B\left[1 \pm C \ln\left(\frac{L}{R}\right)\right],$$

$$\langle D_{y\pm}/\tau\rangle = B\left\{1 \pm C\left[\ln\left(\frac{L}{R}\right) - 1\right]\right\}, \tag{8}$$

where $B=2k_BTb$ has units of a diffusion constant and $C=1/(4\pi\eta_{3D}hb)$ is a nondimensional constant. In the subsequent section we explore the validity of these theoretical expressions for a range of soap films with varying h/d and viscosity η_{3D} of the fluid layer comprising the soap films.

IV. FLOW FIELDS IN SOAP FILMS

Particle motions in the soap films are quantified by measurements of the MSD, $\langle\Delta r^2\rangle$, which is ensemble averaged over all particles in the field of view. Figure 4 (see also Table I) shows the MSD for one particular soap film (solid symbols, see the figure caption for details) plotted against the lag time τ. Also shown in the figure is the corresponding MSD for diffusion in a 3D solution that comprises the fluid layer of the soap film (open symbols). From the figure, it is clear that the MSD is linear with respect to τ, indicating free diffusion. By comparing the two MSDs, it is also evident that diffusion in the soap film (solid circles) is faster than in the corresponding bulk solution (open circles). This makes sense, as the Trapeznikov approximation states that the particle is at an effective interface in contact with bulk air phases. Since the air phase has a significantly lower viscosity than the fluid layer, this speeds the diffusive motion of the particle. Finally, Eq. (4) can be solved to estimate the effective 2D shear viscosity η_{SD} from the slope of the MSD.

TABLE I. Material parameters for the nine soap films described in this paper. η_{3D} (determined from diffusivity measurements in bulk solutions) has an error of ±5%, and values of h and d are certain to within ±2%. The uncertainties in η_{int}, derived from Eqs. (1) and (2), are given in the brackets.

η_{3D} (mPa s)	h (nm)	d (nm)	h/d
(a) 2.3	305	500	0.6
(b) 3.0	640	500	1.3
(c) 6.0	510	500	1.0
(d) 10.0	1340	500	2.7
(e) 25.0	1100	500	2.2
(f) 10.0	780	210	3.7
(g) 25.0	2184	210	10.4
(h) 30.0	2100	210	10.0
(i) 30.0	3000	210	14.3

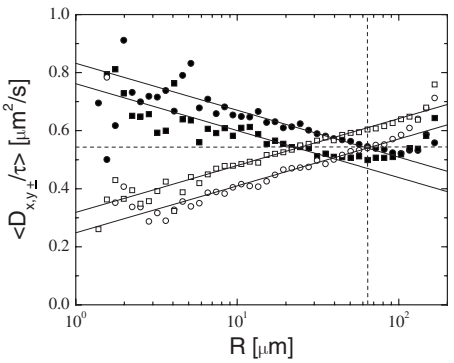

FIG. 5. Correlation functions for the same soap film as in Fig. 4. Symbols are $\langle D_{x+}/\tau\rangle$, solid circles; $\langle D_{x-}/\tau\rangle$, open circles; $\langle D_{y+}/\tau\rangle$, solid squares; $\langle D_{y-}/\tau\rangle$, open squares. Solid lines are fits to the data from Eq. (8), with $B=0.54$ μm^2/s (horizontal dashed line), $C=0.13$, and $L=64$ μm (vertical dashed line).

After the effective 2D shear viscosity has been determined, we attempt to determine the flow fields in this soap film. This is done by looking at the correlated and the anticorrelated motions of pairs of particles, as described in Sec. II B of this paper. The four correlation functions $\langle D_{x+}/\tau\rangle$, $\langle D_{x-}/\tau\rangle$, $\langle D_{y+}/\tau\rangle$, and $\langle D_{y-}/\tau\rangle$ are shown in Fig. 5 as functions of particle separation R. From the figure, it is clear that the correlation functions split around a mean diffusion constant B, with rigid motions (+, solid symbols) being favored and relative motions (−, open symbols) being opposed. Further, the correlation functions vary logarithmically as a function of R, evidenced by the linearity of the data on a logarithmic-linear plot. In fact, the data are well characterized by Eqs. (8), where B, C, and L are fitting parameters. A visual way of determining the fit parameters is by noting that $\langle D_{x+}/\tau\rangle=\langle D_{x-}/\tau\rangle=B$ when $R=L$. Therefore, the dashed horizontal and vertical lines in the figure indicate that $B=0.54$ μm^2/s and $L=64$ μm, while the slope of the four correlation functions simply gives $C=0.13$. These values have been used to fit the four correlation functions with Eqs. 8 in Fig. 5. We should note that the length scale determined above is smaller than the field of view of the microscope and is therefore not subjected to finite-size effects; that is, it truly represents a cutoff length scale for stresses in this particular soap film.

To test the validity of the functional form of the correlation functions, we measure and plot their values for different soap films with a range of 3D viscosities, thicknesses, and tracer particle sizes. This is shown in Figs. 6(a) and 6(b),

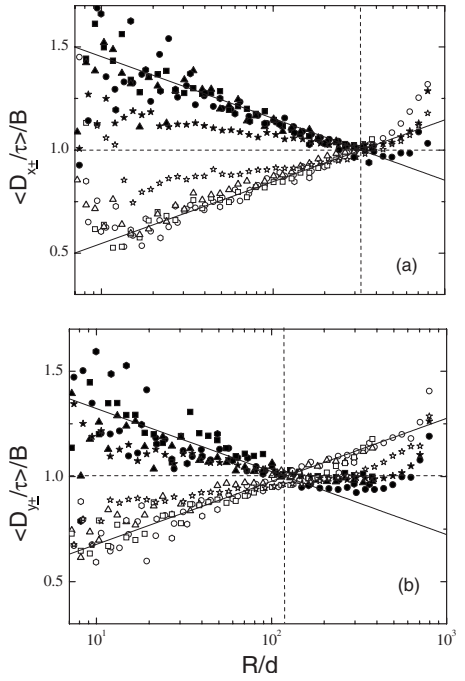

FIG. 6. Scaled (a) longitudinal ($\langle D_{x\pm}/\tau\rangle/B$) and (b) transverse ($\langle D_{y\pm}/\tau\rangle/B$) correlation functions for five soap films plotted against the scaled separation R/d. Solid symbols represent correlated motion while open symbols represent anticorrelated motion. Refer to Table I for details about the soap films. Symbols are triangles, sample (a); hexagons, sample (c); squares, sample (d); circles, sample (f); stars, sample (i). Solid lines are of the form $1\pm C\ln(L/R)$ and $1\pm C[\ln(L/R)-1]$, respectively, based on the values of $C=0.13$ and $L=325d$ that roughly fit the data for the films with $h/d<5$. In particular, sample (i) (stars) is a thicker film with $h/d=14.3$ and those data deviate the most from these straight lines.

where we have nondimensionalized the correlation functions by the scale factor B and the separation R by the particle diameter d for five different soap films, including the one shown in Fig. 5. We find that, for all soap films with $h/d<7$, the longitudinal correlation functions roughly scale onto a single curve that is described by the equation $1\pm 0.13\ln(325d/R)$. For the film where $h/d=14.3$ (stars), there is significant deviation from the scaling, particularly relating to the slope C ($C=0.06$ instead of 0.13). Similarly, the transverse correlation functions for the thin films can be well described by the form $1\pm 0.13[\ln(325d/R)-1]$, while the thicker films again deviate from the scaling (the transverse correlation functions are noisier than their longitudinal counterparts; hence, the deviation is not as clearly visible). The dashed horizontal lines in Figs. 6(a) and 6(b) depict the splitting of the normalized diffusion constants around a value of 1, while the vertical lines are placed at values of $R/d=325$ and $325/e$ (=120) for the longitudinal and the transverse correlation functions, respectively.

Figure 7 shows the fitting parameters from the five soap films described above, along with four additional films. The fit parameter C is plotted against h/d in Fig. 7(a), where we see that $C\approx 0.13$ for all films with $h/d<7\pm 3$, while $C\approx 0.06$ for thicker films. On the other hand, the parameter L/d shown in Fig. 7(b) is nearly constant for all soap films.

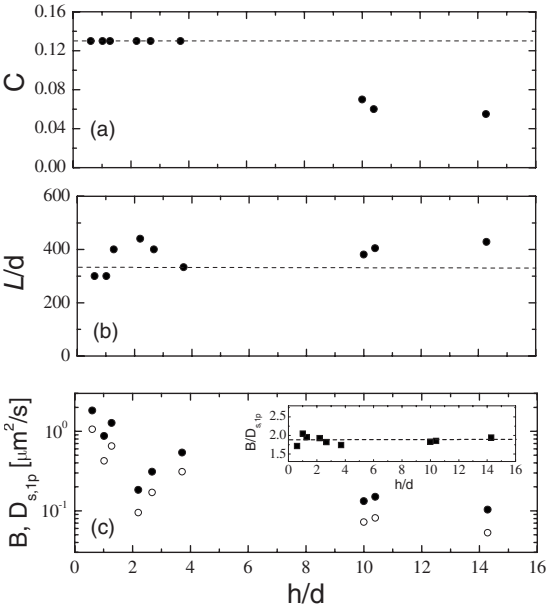

FIG. 7. Fit parameters for nine soap films, including the five shown in Fig. 6, as a function of h/d. (a) C; the dashed line indicates a constant value of 0.13 for all soap films with $h/d<7\pm 3$. (b) L/d; the dashed line represents a value of 325, from the scaling of the correlation functions shown in Fig. 6. (c) B (solid circles) compared to the one-particle diffusion constant $D_{s,1p}$ (open circles). The inset shows the ratio $B/D_{s,1p}$ to be nearly constant with a value of 1.9 ± 0.1.

Finally, in Fig. 7(c) we plot both B and $D_{s,1p}$ as functions of h/d. Neither the fit parameter nor the one-particle diffusion constant shows any discernible trend with h/d; however, they are clearly correlated, and the inset shows that $B/D_{s,1p}\approx 1.9\pm 0.1$ for all soap films. In fact, mathematically we expect $B/D_{s,1p}=2$. This follows from the eigenmobilities of Eqs. (5). In those equations, the eigenmobilities can be thought of as a self-term (the leading term) with a coupling term (the logarithmic term). If the coupling is "removed" then the self-mobility must be recovered and thus b must be proportional to $D_{s,1p}$. Next, consider Eqs. (6), where again the self-mobility must be recovered in the limit of uncorrelated particles. This leads to

$$D_{x\pm}/\tau=\tfrac{1}{2}(2\langle\Delta r_x^2\rangle)/\tau=2D_{s,1p} \tag{9}$$

and likewise for $D_{y\pm}$. By comparison with the self-terms of Eqs. (8), we see that $B=2D_{s,1p}$. Thus, the inset of Fig. 7(c) demonstrates that the one-particle and the two-particle analyses are consistent.

The parameters B and C can be further understood by considering various potentially relevant quantities which all have units of 2D shear viscosity. The first quantity is $\eta_B=\eta_{3D}h$. This product shows up in the theory [Eqs. (5), (7), and (8)] and is an appealing quantity because it depends on two physical parameters that are easy to measure. The second quantity is the effective 2D shear viscosity η_{SD} as determined from the one-particle measurements [Eq. (4)]. The third quantity comes from the Trapeznikov approximation [Eq. (3)], which states that the entire soap film can be con-

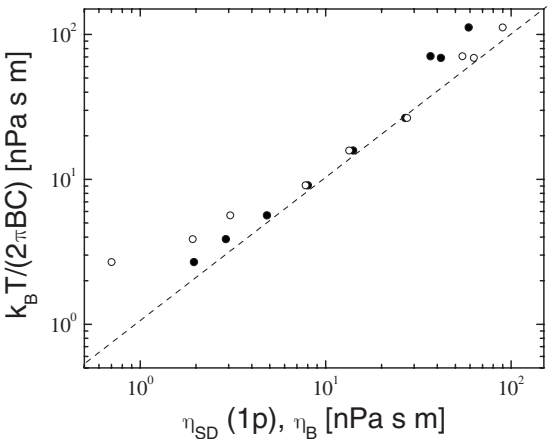

FIG. 8. The scaled quantity $k_BT/(2\pi BC)$ compared to the one-particle effective 2D shear viscosity η_{SD} (solid circles) and η_B (open circles). The dashed line indicates equality between the two quantities.

sidered as an effective interface with a larger 2D shear viscosity $\eta_T=\eta_{3D}h+2\eta_{int}=\eta_B+2\eta_{int}$, thus suggesting that η_T is more relevant than the first quantity η_B. The fourth quantity is the combination $k_BT/(2\pi BC)$, based on the two-particle correlations. From examining the theoretical expressions for the correlation functions described in Eqs. (5), (7), and (8), we see that $B=2k_BTb$ and $C=1/(4\pi\eta_{3D}hb)$, so that $k_BT/(2\pi BC)=\eta_B$. Thus, testing this equality is a test of that theory. In particular, the contribution from η_{int} has not been included in the expression for C, and so it is possible that the theory needs to be modified. We note that the fluid layer in the soap film studied by Di Leonardo *et al.* [4] consisted primarily of glycerol, and presumably η_{int} was irrelevant for their system, that is, $\eta_B\approx\eta_T\gg\eta_{int}$. This is not true for our soap films, as we have situations where $\eta_B\sim\eta_{int}$ as well as $\eta_B\gg\eta_{int}$.

To test these conjectures, we compare three of these quantities in Fig. 8, which shows the scaled quantity $k_BT/(2\pi BC)$ plotted against the measured one-particle effective 2D shear viscosities η_{SD} (solid circles) and η_B (open circles). Each pair of circles at the same vertical position corresponds to one experiment. For thin films with low 2D shear viscosities (lower left corner of the graph), we see that the solid symbols for η_{SD} are to the right of the open symbols for η_B, in agreement with the Trapeznikov approximation. From the difference in these two quantities, one can extract the 2D shear viscosity η_{int}, which we have done previously for these data, finding $\eta_{int}=0.97\pm0.55$ nPa s m [16]. However, for thicker films with higher 2D shear viscosities (top right corner of Fig. 8), we see that the opposite is true; the effective 2D shear viscosities η_{SD} (solid circles) are lower than η_B (open circles), showing that the Saffman-Delbrück equation [Eq. (4)] measures a viscosity that is too low. This occurs even though the thick films still behave as a 2D fluid according to their correlation functions; in other words, Eqs. (5), (7), and (8) still describe the two-particle correlations, albeit with different parameters.

The comparison of η_{SD} and η_B with $k_BT/(2\pi BC)$ in Fig. 8 bolsters these conclusions. For thin films, η_{SD} matches better with $k_BT/(2\pi BC)$ (comparison of solid symbols with the dashed line, lower left of Fig. 8). For thicker films, η_B matches better (comparison of open symbols with the dashed line, upper right of Fig. 8). Our data suggest that in the theory leading to Eqs. (5), (7), and (8), we should replace $\eta_B=\eta_{3D}h$ with η_T. This minor correction would improve the results for thin less viscous films and be negligible for thicker viscous films such as those studied in Ref. [4]. The disagreement between $k_BT/(2\pi BC)$ and η_{SD} shows the breakdown of the applicability of the Saffman-Delbrück equation to extract a useful 2D shear viscosity from one-particle data, for situations with $h/d>7$, and in fact coincides with a breakdown of the equality $\eta_{SD}=\eta_T$ [16].

To summarize, for all films we have $k_BT/(2\pi BC)=\eta_T$ and for thin films we additionally have $\eta_{SD}=\eta_T$. The approximation $\eta_B\approx\eta_T$ is mathematically obvious for thick films, given the definitions of these two 2D shear viscosities. It is worth noting that our prior work suggests that it is necessary to measure η_{SD} (in thin films) to be able to determine η_T, as the viscosity of the surfactant layers η_{int} is usually not known ahead of time [16]; this current work suggests that measuring $k_BT/(2\pi BC)$ is an additional method to obtain η_T and thus η_{int}.

Using these insights, we return to the data shown in Fig. 7. Reconsidering our fit parameters, we can replace η_B with η_T and use $k_BTb=D_{s,1p}$ to get $C=1/(4\pi\eta_Tb)\sim(\eta_TD_{s,1p})^{-1}$. For low values of h/d, Fig. 7(a) shows that C is constant, suggesting that $D_{s,1p}\sim\eta_T^{-1}$ for thin films, as expected [16]. However, for thicker films C decreases, suggesting that b grows faster than η_T^{-1}. Given that Fig. 8 suggests η_T correctly describes thick films, the decrease in C shows that the mobility of particles increases. This again shows that applying the Saffman-Delbrück equation to the one-particle data ($D_{s,1p}$) incorrectly yields a 2D shear viscosity η_{SD} that is too low for the thicker films.

We also note that the parameter L/d is nearly constant for all soap films. This is very surprising, as the logarithmic cutoff in the decay of the correlation functions can arise from three possible factors: (1) finite size of the film, (2) inertial effects, and (3) viscous drag on the soap film from the bulk air phases. The size of the frame used to house the film is of order ~1 cm, which is too large to explain the values of L obtained from fits to the correlation functions. Inertial effects arise at length scales given by $L=\eta_{3D}/\rho U$, where ρ is the fluid density and U is a typical probe particle speed. This gives length scales of order ~1 m, which is again too large to explain our fit-derived length scales. Finally, the viscous cutoff length scale is given by $L=\eta_{SD}/\eta_{air}$. Clearly, as can be seen from Fig. 8, this length scale must increase as the effective 2D shear viscosity increases. Therefore, the near-constant value of L/d for soap films over a range of η_{SD} remains a mystery. Note that none of these potential origins for L would predict any dependence on the particle size d; that is, they might predict a film-independent L but not a constant L/d as we find (from data including two different particle sizes d differing by a factor of 2.4).

One additional particle-based explanation for the constant value of L/d could be capillary effects. Capillary effects arise from deformation of the interface by the particle, with an energy gain obtained when two particles stick to each

other. However, it is not obvious that this moderately short-range interaction would lead to such a very long length scale as we observe ($L/d \sim 325$). We leave the reasons for the constant value of L/d as a question for future research.

V. CONCLUSION

We have used the technique of two-particle microrheology to characterize the flow fields in soap films of varying thickness h, where $0.6 \leq h/d \leq 14.3$ (based on the probe diameter d). In particular, we determine the "eigenmobilities" of thermally correlated motions of probe particles in these soap films. These eigenmobilities consist of correlated motion parallel and perpendicular to the lines joining the centers of pairs of particles and rigid and relative motions as well. The eigenmobilities are found to split around a mean value and decay logarithmically as a function of particle separation for all soap films. The flow fields of all films we observe are well described by theoretical models. A study of the fit parameters shows that thin films have a simple behavior, where a 2D shear viscosity η_T predicted by Trapeznikov over 50 years ago correctly describes both one-particle and two-particle motions [17]. In fact, for the thinnest films, our results suggest that prior theoretical work should be modified slightly to use η_T [4]. In our work we also see a transition from "pure 2D" to "3D-influenced" behavior at $h/d = 7 \pm 3$. For thicker films, two-particle correlations still follow the predicted form for a quasi-2D fluid, with 2D shear viscosity η_T. However, one-particle motion is faster than expected, and other significant deviations from the thin-film behavior are noted. The results of our study on soap films can have important consequences for other 2D systems, including but not limited to microfluidic flow in confined geometries, protein and surfactant monolayers at an air-water interface, and the cell membrane.

ACKNOWLEDGMENTS

Funding for this work was provided by the National Science Foundation (Contract No. DMR-0804174), the Petroleum Research Fund, administered by the American Chemical Society (Contract No. 47970-AC9), and the University Research Committee of Emory University. We thank J. Gallivan for the use of the spectrophotometer and H. Diamant, H. A. Stone, E. van Nierop, and M. Hopson for helpful discussions.

[1] H. A. Stone and A. Ajdari, J. Fluid Mech. **369**, 151 (1998).
[2] A. J. Levine and F. C. MacKintosh, Phys. Rev. E **66**, 061606 (2002).
[3] T. M. Fischer, J. Fluid Mech. **498**, 123 (2004).
[4] R. Di Leonardo, S. Keen, F. Ianni, J. Leach, M. J. Padgett, and G. Ruocco, Phys. Rev. E **78**, 031406 (2008).
[5] C. Cheung, Y. H. Hwang, X-l. Wu, and H. J. Choi, Phys. Rev. Lett. **76**, 2531 (1996).
[6] J. Mathé, J. M. Di Meglio, and B. Tinland, J. Colloid Interface Sci. **322**, 315 (2008).
[7] B. Martin and X. I. Wu, Rev. Sci. Instrum. **66**, 5603 (1995).
[8] P. Vorobieff and R. E. Ecke, Phys. Rev. E **60**, 2953 (1999).
[9] J. C. Crocker, M. T. Valentine, E. R. Weeks, T. Gisler, P. D. Kaplan, A. G. Yodh, and D. A. Weitz, Phys. Rev. Lett. **85**, 888 (2000).
[10] A. J. Levine and T. C. Lubensky, Phys. Rev. Lett. **85**, 1774 (2000).
[11] M. L. Gardel, M. T. Valentine, J. C. Crocker, A. R. Bausch, and D. A. Weitz, Phys. Rev. Lett. **91**, 158302 (2003).
[12] L. Starrs and P. Bartlett, J. Phys.: Condens. Matter **15**, S251 (2003).
[13] B. R. Dasgupta and D. A. Weitz, Phys. Rev. E **71**, 021504 (2005).
[14] A. W. C. Lau, B. D. Hoffmann, A. Davies, J. C. Crocker, and T. C. Lubensky, Phys. Rev. Lett. **91**, 198101 (2003).
[15] V. Prasad, S. A. Koehler, and E. R. Weeks, Phys. Rev. Lett. **97**, 176001 (2006).
[16] V. Prasad and E. R. Weeks, Phys. Rev. Lett. **102**, 178302 (2009).
[17] A. A. Trapeznikov, *Proceedings of the 2nd International Congress on Surface Activity* (Butterworths, London, 1957), p. 242.
[18] J. C. Crocker and D. G. Grier, J. Colloid Interface Sci. **179**, 298 (1996).
[19] P. Dhar, V. Prasad, E. R. Weeks, T. Bohlein, and T. M. Fischer, J. Phys. Chem. B **112**, 9565 (2008).
[20] T. G. Mason, A. Dhople, and D. Wirtz, MRS Proceedings on Statistical Mechanics in Physics and Biology (Materials Research Society, Pittsburgh, 1997), Vol. 463, p. 153.
[21] P. D. T. Huibers and D. O. Shah, Langmuir **13**, 5995 (1997).
[22] P. G. Saffman and M. Delbrück, Proc. Natl. Acad. Sci. U.S.A. **72**, 3111 (1975).
[23] B. X. Cui, H. Diamant, B. H. Lin, and S. A. Rice, Phys. Rev. Lett. **92**, 258301 (2004).
[24] H. Diamant, B. Cui, B. Lin, and S. A. Rice, J. Phys.: Condens. Matter **17**, S2787 (2005).